DISPLACEMENT MEASURING INTERFEROMETRY MEASUREMENT UNCERTAINTY

Mike Holmes, Chris Evans
Zygo Corporation, Middlefield, CT 06455

Introduction

Displacement measuring interferometry is a key enabling technology allowing the semiconductor industry to continue to shrink linewidths by a factor of two every 2-3 years and increase integrated circuit performance. Intel, for example, have indicated that they expect to see limited production at the 65 nm node in 2005; line widths down to 32 nm by the end of the decade are predicted in the most recent ITRS roadmap. Typically, overlay budgets are about 1/3 the linewidth and reticle and wafer stage metrology themselves are but one of many factors contributing to overlay budget. Hence it is clear that sub-nm wafer stage position uncertainties will be needed on the stages in the lithography tools used to make the integrated circuits.

Nanometer class position uncertainties are required in other applications, such as a long travel measuring system being developed at Zygo. In this application, the position of a 6 degree of freedom stage with a working volume of 500 x 1 x 1 mm must be known with an uncertainty of 1 nm (k=1). Including calibration tools and the wavelength tracker, 14 DMIs are used in four different configurations. This presentation focuses on one of those configurations, and gives a detailed analysis of the uncertainties; the methodology is shown here for two uncertainty contributors.

Ideal

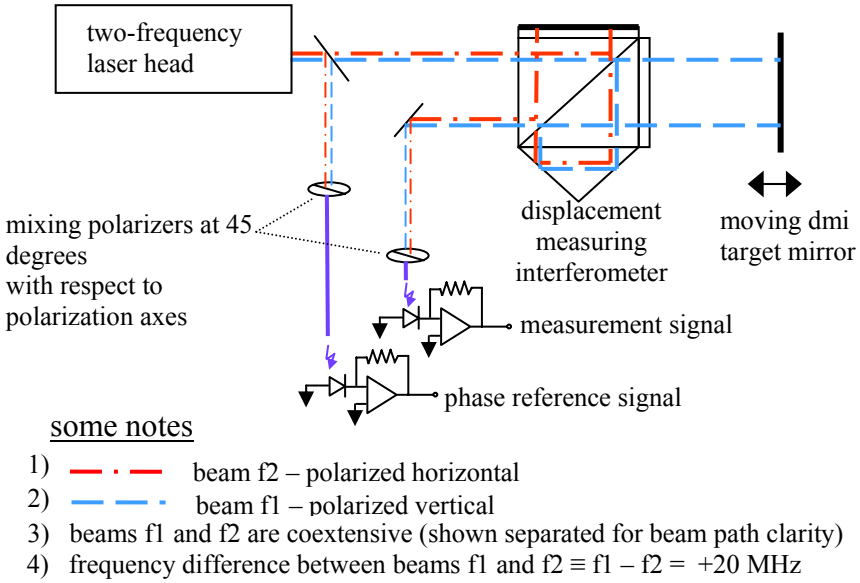

Figure 1 – Ideal heterodyne displacement measuring interferometer system minus phase interpolator

Figure 1 shows an idealized heterodyne Displacement Measuring Interferometer (DMI) system[1,2] consisting of the laser head, displacement measuring interferometer, moving target mirror, and transimpedance amplifiers. The output from the laser head is two coextensive linearly polarized beams ($\lambda_{1,2} \approx 632.991$ nm) which are separated in frequency by 20 MHz. The polarization states are orthogonal to each other. The two components are separated in the interferometer. One component travels a constant optical path through the reference arm of the interferometer while the other travels through the measurement arm whose optical path length is dependent upon the position of the target mirror. The two components rejoin inside the interferometer and are mixed and directed onto the measurement signal transimpedance amplifier. The electrical output from this amplifier is a 20 MHz ± Doppler shift (a Doppler shift occurs when the target mirror is moving and is proportional to its velocity) sinusoid. This signal's magnitude is

proportional to the heterodyne signal optical power and its phase is proportional to the interferometer's measurement arm optical path length. The electrical phase reference signal is generated from a portion of the interferometer's input beams. Note that this signal has constant phase as the two components are traveling a common constant optical path prior to being mixed and directed onto the phase reference transimpedance amplifier. Not shown in this figure, the phase interpolator measures changes in phase between the phase reference signal and the measurement signal and calculates the displacement of the target mirror. In our ideal DMI system, a change in phase between these two signals occurs as the interferometer's measurement arm path length only changes with the moving target.

Real

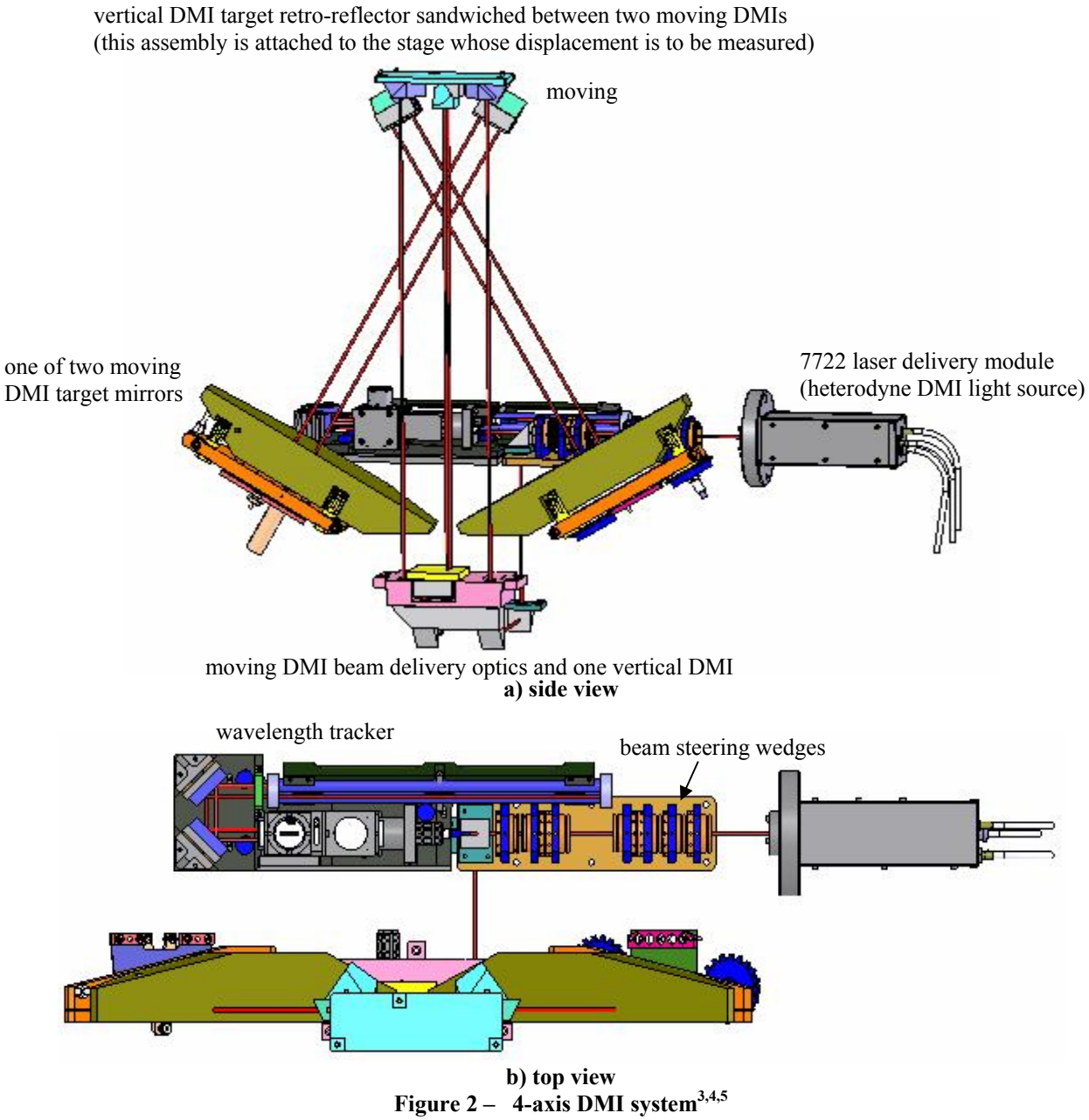

Figure 2 – 4-axis DMI system[3,4,5]

In reality there are many sources of changing phase of the measurement signal other than target mirror displacement[6]. These other sources contribute to measurement uncertainty and include wavelength instability, beam purity, measurement arm refractive index instability, reference arm refractive index instability, interferometer beam mixing/stray light, wavefront deformation/beam shear, and phase interpolator noise.

Figure 2 shows one of the subsystems – in this case a 4-axis DMI system. The heterodyne DMI light source is a Zygo 7722 laser delivery module[7]. This fiber-fed laser module outputs more than of 1 mW of optical energy while generating less than 20 mW of heat. The output is exactly as described in the previous section with beam purity of 32 ppm (i.e., 32 parts of beam component number 1 with a polarization state matching that of beam component number 2 per 1000000 parts of beam component number 1) and a wavelength instability of <1 ppb over any 1 hour period of time (<1 part-per-billion of the nominal wavelength). The delivery module's optical output is directed to the 4-axes of DMI (3 DMIs and 1 wavelength tracker) via a set of steering wedges. Immediately following the steering wedges, 25% of the beam is allowed to pass to the wavelength tracker while the remaining 75% of the beam is directed downwards to a set of beam steering optics including two right-angle prisms and two rhomboid prisms. The rhomboids split the beam into three beams of "equal" power. One of the beams is directed into a "vertical" DMI while the other two are directed into two "moving" DMIs. Note that in this DMI system the two moving interferometers are moving with the stage motion while their target mirrors are "stationary". The vertical DMI has a target retro-reflector which moves with the moving interferometers. All three DMIs see a change in the optical path lengths of their measurement arms with vertical motion of the stage to which they are attached (not shown in Figure 2) while only the two moving DMIs see a change in their measurement arm optical path lengths with lateral motions of the stage. With this subsystem we have redundant measurements of the vertical motions of the stage with three distinct optical paths and redundant measurements of the lateral motions with two distinct optical paths. For the purposes of this presentation/abstract, only the measurement uncertainty of one of the moving DMIs will be considered. Further, the measurement uncertainty will be considered in the coordinate frame of the interferometer, not the machine coordinate frame.

The moving DMI

The moving DMI will be operating in a vacuum (about 2 mbar) with a maximum interferometer vertical displacement of 500 mm. The measurement uncertainty is tabulated in Table 1. For the sake of brevity, only measurement uncertainties stemming from interferometer thermal sensitivity and beam sheering of non-planar wavefronts will be considered with some detail here.

uncertainty source	contribution to DMI measurement uncertainty
laser head: beam component purity	0.05 nm
wavelength instability	0.20 nm
moving DMI: thermal sensitivity	0.05 nm
beam mixing/stray light	0.10 nm
beam shear	0.60 nm
phase interpolation electronics	0.15 nm
vacuum index uncertainty	0.32 nm
Total (RSS):	0.73 nm

Table 1- Moving DMI measurement uncertainty (1σ)

Figure 3 shows the moving interferometer. The reference arm is shown in Figure 3.b while the measurement arm is shown in 3.c. As this interferometer expands and contracts with temperature, it will grow and shrink into and out of the measurement arm some distance proportional to a length and change in temperature. The length used for this calculation is shown in Figure 3.d and is referred to as $l_{sensitive}$. What we need to do here is to calculate the temperature sensitivity of the optical path length difference between the reference and measurement arms. The optical path length difference is given by

$$OPD = n_{ref} \cdot l_{ref} - n_{meas} \cdot l_{meas}$$

where OPD is the optical path length difference between the reference and measurement arms, n_{ref} is the reference arm's index, l_{ref} is the reference arm physical length, n_{meas} is the measurement arm's index, and l_{meas} is the measurement arm physical length. Since the measurement arm consists of both glass and vacuum, it is useful to re-write the equation for optical path length difference as

$$OPD = n_{SiO2} \cdot l_{ref} - n_{SiO2} \cdot l_{meas\_g} - n_{v} \cdot l_{meas\_v}$$

where n_{SiO2} is the index of the fused silica, n_v is the index of the vacuum, l_{meas_g} is the measurement arm's physical length in glass, and l_{meas_v} is the measurement arm's physical length in vacuum.

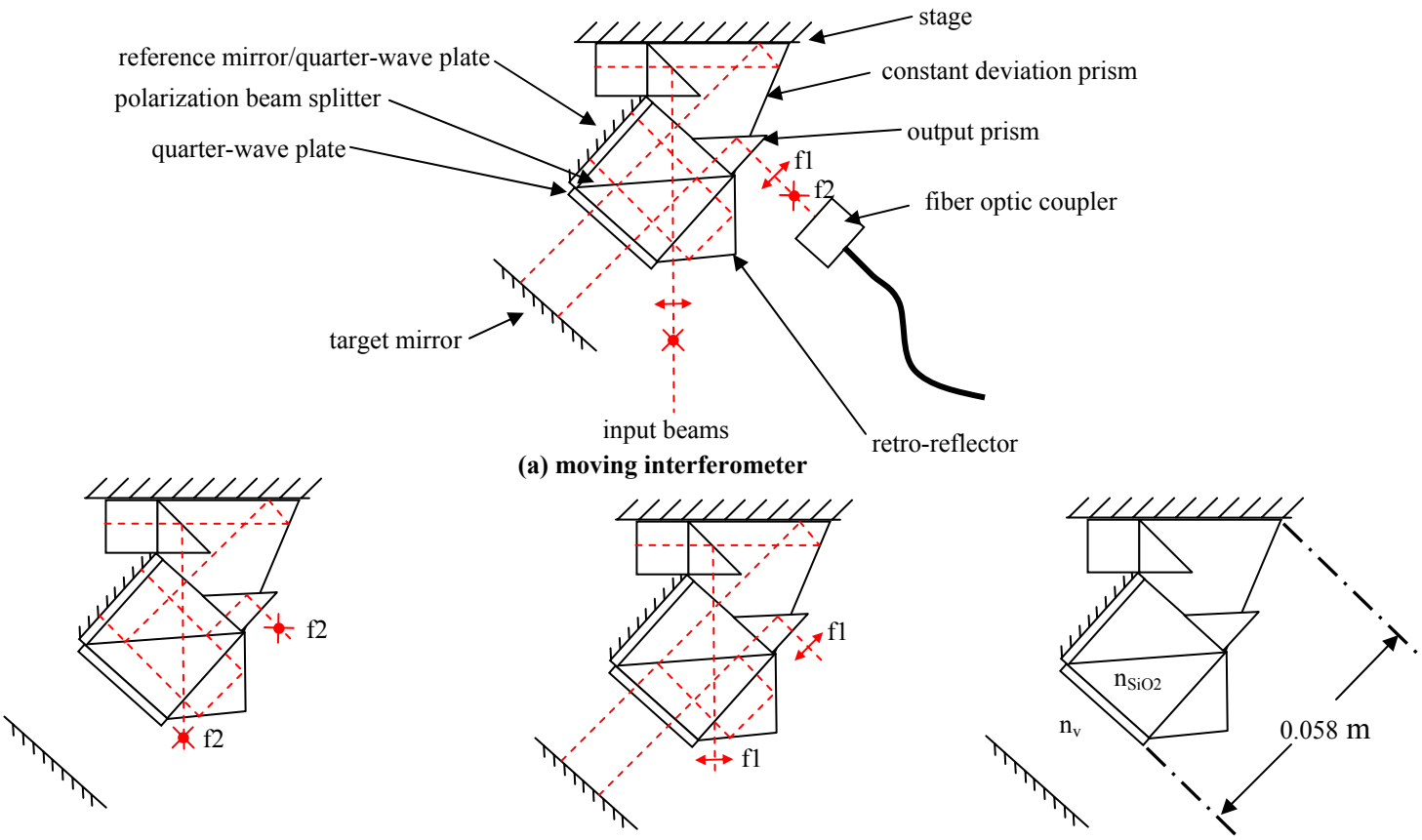

(a) moving interferometer

(b) reference arm **(c) measurement arm** **(d) details of interest**

Figure 3 – Moving interferometer schematic diagrams

To find the temperature sensitivity of the interferometer we must solve

$$\frac{d(OPD)}{dT} = \frac{d(n_{SiO2} \cdot l_{ref} - n_{SiO2} \cdot l_{meas\_g} - n_v \cdot l_{meas\_v})}{dT}$$

$$= n_{SiO2}(l_{ref} - l_{meas\_g})\alpha_{SiO2} + (l_{ref} - l_{meas\_g})\frac{d(n_{SiO2})}{dT} - n_v(4 \cdot l_{sensitive})\alpha_{SiO2} - l_{meas\_v}\frac{d(n_v)}{dT}.$$

We ignore the last term in the equation above since measurement uncertainty due to index variations will be considered/budgeted in the analysis of the wavelength tracker. The input parameters used to solve the above equation are given in Table 2.

model input	description	expectation	standard uncertainty
n_{SiO2}	index of the fused silica	1.45698	0.000012
$d(n_{SiO2})/dT$	thermal coefficient for the index of fused silica	8.3 ppm °C^{-1}	0.3 ppm °C^{-1}
α_{SiO2}	thermal expansion coefficient for fused silica	0.55 ppm °C^{-1}	0.02 ppm °C^{-1}
n_v	index in the vacuum	1.000001327	7.78 x 10^{-9}
l_{ref}	reference arm physical path length (m)	0.270 m	0.0007 m
l_{meas_g}	measurement arm physical glass path length (m)	0.270 m	0.0007 m
$l_{sensitive}$	sensitive length to thermal growth of interferometer affecting l_{meas_v} (m)	0.058 m	0.0007 m
T	temperature (°C)	23 °C	0.0014 °C
P	pressure (Torr)	3.75 Torr	0.022 Torr
F	partial pressure of the water vapor in the vacuum (Torr)	0 Torr	0 Torr

Table 2 – Model input parameter expected values and standard uncertainties

Plugging in the expected values given in the table above yields an expected interferometer temperature sensitivity of $X_{\frac{d(OPD)}{dT}} = 127.6 \text{ nm °C}^{-1}$.

The corresponding standard uncertainty is

$$U_{\frac{d(OPD)}{dT}} = \left(\left(\frac{\partial(\frac{d(OPD)}{dT})}{\partial n_{SiO2}} \right)^2 U_{n_{SiO2}}^2 + \left(\frac{\partial(\frac{d(OPD)}{dT})}{\partial n_v} \right)^2 U_{n_v}^2 + \left(\frac{\partial(\frac{d(OPD)}{dT})}{\partial l_{ref}} \right)^2 U_{l_{ref}}^2 + \left(\frac{\partial(\frac{d(OPD)}{dT})}{\partial l_{meas\_g}} \right)^2 U_{l_{meas\_g}}^2 + \left(\frac{\partial(\frac{d(OPD)}{dT})}{\partial l_{sensitive}} \right)^2 U_{l_{sensitive}}^2 + \left(\frac{\partial(\frac{d(OPD)}{dT})}{\partial \alpha_{SiO2}} \right)^2 U_{\alpha_{SiO2}}^2 + \left(\frac{\partial(\frac{d(OPD)}{dT})}{\partial(\frac{d\,n_{SiO2}}{dT})} \right)^2 U_{\frac{d\,n_{SiO2}}{dT}}^2 \right)^{\frac{1}{2}}$$

$$= 11.5 \text{ nm } ^\circ\text{C}^{-1} \ .$$

The uncertainties in glass path length, vacuum path length, and the sensitive ($l_{sensitive}$) length of the interferometer dominate the standard uncertainty. The worst case optical path difference temperature sensitivity is 139.1 nm °C^{-1}. Note that this sensitivity has been calculated for the total optical path difference between the reference and measurement arms of the interferometer. Since there are 2 passes to the target mirror in the measurement arm, this number must be divided by 4 to get the measurement sensitivity. Next we multiply the measurement sensitivity by our temperature uncertainty to yield the resulting, conservative, moving DMI measurement uncertainty (1σ) of 0.05 nm.

Beam shear of distorted wavefronts

Some shearing of the measurement arm beam with respect to the reference arm beam within the moving interferometer will occur with changes in stage orientation. Based on the specifics of the application/design, it has been determined that this beam shear will not exceed 0.2 mm. If the measurement and reference arm beam wavefronts were planar perpendicular to the direction of their propagation, then there would be no change in the phase of the heterodyne signal as the measurement arm beam wavefront shears across the reference arm beam wavefront. However, Gaussian beam wavefronts are more spherical than planar. The wavefront departure from planar further increases as the wavefront passes through components in its optical path with inhomogeneous optical properties resulting in parts of the wavefront seeing differing indices than other parts of the wavefront thereby resulting in phase delays across the wavefront, changing its shape. As the non-planar wavefronts are sheared, there is a resulting change in phase of the heterodyne signal which is generated by mixing the electric fields on the face of a fast photodiode and whose phase is the summation of all the little phase differences between the two interfering wavefronts. For modeling purposes, we assume that all beams are Gaussian with complex amplitudes and are well represented by the equation (suppressing the time-dependence of phase)

$$E = \frac{E_0 i z_0}{z + i z_0} \exp\left[-i \frac{n 2\pi}{\lambda} \left(\frac{x^2 + y^2}{2\left(z + i z_0\right)} + z \right) \right]$$

where E_0 is the electric field amplitude, Z_0 is the Raleigh distance, n is the index, $2\pi\lambda^{-1}$ is the wave number, and x, y, and z are the Cartesian coordinates. Note that the light is propagating in the z-direction. Since our beams are round in cross-section, I note that

$$x = r \cdot \cos(\theta), \ y = r \cdot \sin(\theta), \text{ and } r^2 = x^2 + y^2$$

where r is beam radius and θ is the θ_z. Ultimately we will multiply the sum of the measurement arm beam's electric field and the reference arm beam's electric field with its complex conjugate to get a measurement beam signal. This intensity distribution will be integrated over the active area of the detector to determine the net phase of the signal. Said another way,

$$E_{ref} = \frac{E_0 i z_0}{z_{ref} + i z_0} \exp\left[-i \frac{n_{ref} 2\pi}{\lambda_{ref}} \left(\frac{r_{ref}^2}{2\left(z_{ref} + i z_0\right)} + z_{ref} \right) \right],$$

$$E_{meas} = \frac{E_0 i z_0}{z_{meas} + i z_0} \exp\left[-i \frac{n_{meas} 2\pi}{\lambda_{meas}} \left(\frac{r_{meas}^2}{2\left(z_{meas} + i z_0\right)} + z_{meas} \right) \right], \text{ and}$$

$$I(r,\theta) = \int_0^{2\pi}\int_0^{r}\left(E_{meas}+E_{ref}\right)\left(E_{meas}+E_{ref}\right)^{*} r\,dr\,d\theta .$$

We now use a phase-shifting algorithm to extract phase information from the measurement beam signal, which is proportional to the intensity described by the equation above. In this way we can predict changes in phase that result from beam shearing of the non-planar wavefronts. The magnitude of the DMI measurement error that results from beam shear is a strong function of the shapes of the wavefronts that are being sheared. One can modify the electric field equation to look like

$$E = \frac{E_0 iz_0}{z+iz_0}\exp\left[-i\frac{n2\pi}{\lambda}\left(\frac{shape(x,y)}{2\left(z+iz_0\right)}+z\right)\right]$$

where shape(x, y) is a function describing a shape. The really ambitious person could then investigate sensitivities to wavefront shape. It turns out that our wavefronts are predominantly spherical (i.e., $shape(x,y) = x^2 + y^2$).

moving DMI component	number of passes	specification	expected value	uncertainty
CDP base prism	1	0.02 λ PV	0.015 λ PV	0.003 λ PV
CDP launch	1	0.02 λ PV	0.015 λ PV	0.003 λ PV
PBS cube	4	0.02 λ PV	0.015 λ PV	0.003 λ PV
retro-reflector	1	0.02 λ PV	0.015 λ PV	0.003 λ PV
measurement window/reference mirror	4	0.02 λ PV	0.015 λ PV	0.003 λ PV
output prism	1	0.02 λ PV	0.015 λ PV	0.003 λ PV
steering wedges	6	0.02 λ PV	0.015 λ PV	0.003 λ PV
right angle prism	1	0.02 λ PV	0.015 λ PV	0.003 λ PV
Rhomboid	2	0.02 λ PV	0.015 λ PV	0.003 λ PV
fold mirror	2	0.125 λ PV	0.094 λ PV	0.018 λ PV
delivery module	1	0.02 λ PV	0.015 λ PV	0.003 λ PV
total			**0.518 λ PV**	**0.029 λ PV**

Table 3 – Moving DMI component level wavefront distortion specifications

The moving DMI component-level wavefront distortion specifications are given in Table 3. Note that the expected values for the component-level wavefront distortion specifications are assumed correlated as all of the optical components are subjected to similar manufacturing processes. Using the values in Table 3, the measurement error resulting from a 0.2 mm beam shear of the measurement arm beam with respect to the reference arm beam is 0.60 ± 0.04 nm.

Conclusions

Uncertainty analysis plays a vital role in capturing/bounding sources of uncertainty and provides the means by which a successful design can be realized. In this extended abstract, we provide an overview of our approach to reach nanometer level measurement uncertainty with heterodyne displacement measuring interferometry.

References

1) Zygo Corporation, "Displacement Measuring Interferometry Primer," www.zygo.com, Jan 1999.
2) A. Slocum, "Precision Machine Design," Prentice Hall, Englewoods Cliffs, NJ, 1992.
3) Henry Allen Hill, "Apparatus for generating linearly orthogonally polarized light beams," U.S. Patent No. 6157660, Dec. 5, 2000.
4) Van Doren, Kuechel, and Evans, "Metrology system for precision 3D motion," U.S. Patent App. 20030223078, Dec. 4, 2003.
5) Evans and Zanoni, "Apparatus and methods for high accuracy metrology and positioning of a body," U.S. Patent App. 20030112445, June 19, 2003.
6) A.E. Rosenbluth and N. Bobroff, "Optical sources of nonlinearity in heterodyne interferometers," Precision Engineering, 12, 7-11, 1990.
7) Zygo Corporation, "ZMI 7722 Laser Source," Operator's Manual OMP-0475A, www.zygo.com, Jan 1999.

Acknowledgements

This work is based on analytical techniques developed at Zygo Corporation over an extended period of time. Some of the key people contributing to these techniques are Dr. Henry Hill, Dr. Peter de Groot, Lars Selberg, Michael Schroeder, and Mike Metz.